Available online at www.sciencedirect.com
SCIENCE DIRECT®
Synthetic Metals 151 (2005) 285–292
SYNTHETIC METALS
www.elsevier.com/locate/synmet

Bis(2,2-diphenylvinyl)spirobifluorene: An efficient and stable blue emitter for electroluminescence applications

Fang-Iy Wu [a], Ching-Fong Shu [a,*], Tsai-Te Wang [a], Eric Wei-Guang Diau [a,*], Chin-Hsiung Chien [b], Chang-Hao Chuen [b], Yu-Tai Tao [b,*]

[a] *Department of Applied Chemistry, National Chiao Tung University, Hsin-Chu 30035, Taiwan*
[b] *Institute of Chemistry, Academia Sinica, Taipei 11529, Taiwan*

Received 7 March 2005; accepted 10 June 2005
Available online 5 July 2005

Abstract

We have synthesized a spirobifluorene-based **DPVBi** [4,4′-bis(2,2-diphenylvinyl)-1,1′-biphenyl] analogue, **DPVSBF** [2,7-bis(2,2-diphenylvinyl)-9,9′-spirobifluorene], in which the bis(2,2-diphenylvinyl) groups are connected through the 2 and 7 positions of the spirobifluorene framework, and have characterized its thermal properties, electronic properties (viz. absorption and photoluminescence), and electrochemical behavior. The presence of the rigid spirobifluorene linkage imparts significant improvement in the material's glass transition temperature and morphological stability, while preserving most of the photophysical and electronic properties of its non-spiro, biphenyl analogue, **DPVBi**. Organic electroluminescent devices having the structure ITO/NPB/**DPVSBF**/AlQ/LiF/Al display bright emissions with a λ_{max} at 474 nm (CIE coordinates: 0.16, 0.24) and exhibit maximum luminescence exceeding 40,000 cd/m^2. At a driving current density of 100 mA/cm^2 (6.4 V), a luminance of 4110 cd/m^2 was obtained with external quantum efficiency of 2.54%, luminance efficiency of 4.1 cd/A, and power efficiency of 2.0 lm/W. Moreover, the **DPVSBF**-based device exhibits a 16-fold enhancement in the operation lifetime relative to that of a similar device based on **DPVBi**.

Keywords: Spirobifluorene; Glass transition temperature; Blue emission; Lifetime; OLED

1. Introduction

Since their discovery by Tang et al. [1] research into multi-layered organic light-emitting diodes (OLEDs) has been actively pursued because of their potential applications in flat-panel displays [2]. Considerable attention has been directed toward the development of new conjugated organic materials that function as efficient light emitters and/or charge transporters [3]. Organic light-emitting materials having large band-gap energies, which emit blue light efficiently, are of particular interest, because they are desired for use as blue light sources in full-color display applications. In addition, they are able to serve as energy-transfer donors in the presence of lower-energy fluorophores [4]. Recently, efficient organic blue- and white-light-emitting diodes have been prepared by utilizing a blue-emitting distyrylarylene derivative, 4,4′-bis(2,2-diphenylvinyl)-1,1′-biphenyl (**DPVBi**), to function as the electroluminescent layer [5,6]. The active emitting material in these devices is characterized by its high solid-state photoluminescence efficiency. Amorphous films of **DPVBi** fabricated by vacuum evaporation have a tendency, however, to crystallize [7]. This inherent problem presents a limitation for its LED applications because crystal formation destroys film homogeneity and crystal boundaries raise the resistance of the sample, which eventually leads to device failure [8].

Amorphous materials that possess high T_g values are often less vulnerable to heat-induced morphological changes and this characteristic makes them more desirable for fabricating molecular LEDs [8,9]. Our goal was to attain a material that resembles **DPVBi** in its electroluminescence

* Corresponding authors. Tel.: +886 35 712121; fax: +886 35 723764.
E-mail address: shu@cc.nctu.edu.tw (C.-F. Shu).

0379-6779/$ – see front matter © 2005 Elsevier B.V. All rights reserved.
doi:10.1016/j.synthmet.2005.06.003

and charge transport properties, but possesses a significantly higher glass transition temperature and a reduced tendency toward crystallization. Herein, we report the synthesis of a spirobifluorene-based **DPVBi** analogue, **DPVSBF**, in which the two 2,2-diphenylvinyl groups are connected at the 2 and 7 positions of the spirobifluorene framework. Because the spirobifluorene linkage enhances molecular rigidity and hinders close packing and intermolecular interactions, we expected the glass transition temperature to increase and the tendency for crystallization to reduce [10,11]. In addition, most of the desired electronic and optical properties of the corresponding biphenyl molecule will remain substantially unchanged because of the tetrahedral nature of the carbon atom at the spiro center, which connects the conjugated moieties through a σ-bonded network [12]. Molecular weight is another limiting factor that must be considered when designing materials for OLED applications: molecules that have very high molecular weights tend to be difficult to evaporate – they may even decompose – during the thermal evaporation used to deposit materials in the OLED fabrication process. The low molecular weight of **DPVSBF**, relative to that of 2,2′,7,7′-tetrakis(2,2-diphenylvinyl)-9,9′-spirobifluorene (**Spiro-DPVBi**) [13], leads to its lower sublimation temperature. In fact, **DPVSBF** can be sublimed smoothly in a vacuum chamber without thermal decomposition, whereas the sublimation conditions required for **Spiro-DPVBi** are quite harsh [13a]. We have prepared electroluminescent devices based on **DPVSBF** and have compared them with those based on **DPVBi**. Besides a bright blue emission with similar or better performance characteristics, we observed a significant improvement in device lifetime when using **DPVSBF**. The morphological stability is believed to contribute to the extended lifetime.

2. Experimental

2.1. General directions

4,4′-Bis(2,2-diphenylvinyl)-1,1′-biphenyl (**DPVBi**) [14], 2,2-diphenylvinyl bromide (**1**) [15], and 2,7-dibromo-9,9′-spirobifluorene (**3**) [16] were synthesized as reported previously. The solvents were dried using standard procedures. All other reagents were used as received from commercial sources, unless otherwise stated. Differential scanning calorimetry (DSC) was performed on a SEIKO EXSTAR 6000DSC unit at a heating rate of 20 °C min^{-1} and a cooling rate of 40 °C min^{-1}. Samples were scanned from 30 to 400 °C, cooled to 0 °C, and then scanned again from 30 to 400 °C. The glass transition temperatures (T_g) were determined from the second heating scan. Thermogravimetric analysis (TGA) was undertaken on a DuPont TGA 2950 instrument. The thermal stability of the samples under a nitrogen atmosphere was determined by measuring their weight loss while heating at a rate of 20 °C min^{-1}. UV–vis spectra were measured using an HP 8453 diode-array spectrophotometer. Photoluminescence (PL) spectra were obtained on a Hitachi F-4500 luminescence spectrometer. Cyclic voltammetry (CV) measurements were performed using a BAS 100 B/W electrochemical analyzer. The oxidation and reduction measurements were undertaken, respectively, in anhydrous CH_2Cl_2 and anhydrous THF, containing 0.1 M $TBAPF_6$ as the supporting electrolyte, at a scan rate of 50 mV s^{-1}. The potentials were measured against an Ag/Ag^+ (0.01 M $AgNO_3$) reference electrode using ferrocene as the internal standard.

2.2. Picosecond time-resolved measurements

Picosecond time-resolved experiments were performed using a time-correlated single photon counting (TCSPC) system (Fluotime 200, PicoQuant). The excitation laser pulse at 375 nm (LDH375, PicoQuant) was focused onto a l-cm-thick cuvette containing the sample solution. The fluorescence emitted at a right angle to the pulse was collected by a lens pair, a double monochromator (f/3.2, subtractive type), and a multi-channel plate photomultiplier detector (R3809U-50, Hamamatsu). A polarizer was used to select the polarization of the emission with respect to the excitation laser pulse; in all experiments reported here, the polarization was fixed at the magic angle condition (54.7°). The full width at half maximum (FWHM) of the instrument response function (IRF) was determined prior to each measurement to be ca. 70 ps.

2.3. 2-(2,2-Diphenylvinyl)-4,4,5,5-tetramethyl-1,3,2-dioxaborolane (2)

n-Butyllithium in hexane (2.5 M, 40 mL) was added slowly under nitrogen to a stirred solution of 2,2-diphenylvinyl bromide (13.0 g, 50.2 mmol) in THF (80 mL) at −78 °C and then the mixture was stirred further for 2 h. *n*-Butyl borate (30 mL, 111 mmol) was added at −78 °C before the mixture was warmed slowly to room temperature and stirred overnight. Water (50 mL) was added, followed by conc. HCl to acidify the mixture (to pH 2), which was then stirred for 2 h. The reaction mixture was extracted with EtOAc and the combined organic phases were dried over $MgSO_4$. Concentration under reduced pressure gave 2,2-diphenylvinyl boronic acid, which, without further purification, was reacted with pinacol (8.50 g, 72.0 mmol) in benzene (100 mL) under reflux for 3 h to effect condensation by the azeotropic removal of the water formed. The mixture was concentrated under reduced pressure and the residue was purified by column chromatography (hexane/EtOAc) to afford **2** (7.53 g, 49%). ^{1}H NMR (300 MHz, $CDCl_3$): δ 1.18 (s, 12H), 6.03 (s, 1H), 7.28–7.36 (m, 10H). ^{13}C NMR (75 MHz, $CDCl_3$): δ 24.7, 83.2, 127.6,127.7, 128.0, 128.1, 129.9, 141.9, 143.2, 159.9. HRMS [M^+]: calcd. for $C_{20}H_{23}BO_2$, 306.1791; found 306.1796.

2.4. 2,7-Bis(2,2-diphenylvinyl)-9,9′-spirobifluorene (DPVSBF)

A mixture of **2** (11.6 g, 37.9 mmol) and 2,7-dibromo-9,9′-spirobifluorene (**3**; 6.50 g, 13.7 mmol), Aliquat 336 (1.00 g), 2.0 M aqueous K_2CO_3 (20 mL), and toluene (60 mL) was degassed and then tetrakis(triphenylphosphine)palladium (197 mg, 1.25 mol%) was added in one portion under nitrogen. After heated at 90 °C for 8 h, the reaction mixture was poured into methanol (300 mL). The precipitate was washed with water and methanol, purified by recrystallization from EtOAc/THF (5:1), and then sublimed to yield **DPVSBF** (5.10 g, 55.4%). ^{1}H NMR (300 MHz, $CDCl_3$): δ 6.12 (d, J = 1.3 Hz, 2H), 6.57 (d, J = 7.6 Hz, 2H), 6.78 (s, 2H), 6.90–7.02 (m, 12H), 7.06 (ddd, J = 7.5, 7.5, 1.0 Hz, 2H), 7.15–7.22 (m, 10H), 7.31 (ddd, J = 7.5, 7.5, 1.0 Hz, 2H), 7.49 (d, J = 7.8 Hz, 2H), 7.69 (d, J = 7.58 Hz, 2H). ^{13}C NMR (75 MHz, $CDCl_3$): δ 65.4, 119.5, 119.8, 124.0, 125.1, 127.3, 127.4, 127.7, 128.1, 128.2, 128.4, 129.4, 129.9, 137.0, 140.0, 140.1, 141.6, 142.3, 143.2, 148.2, 148.8. HRMS $[M+H]^+$: calcd. for $C_{53}H_{36}$, 672.2817; found 672.2815. Anal. Calcd. for $C_{53}H_{36}$: C, 94.60; H, 5.40. Found: C, 94.61; H, 5.42.

2.5. Fabrication of light-emitting devices

The hole-transport material 4,4′-bis[*N*-(1-naphthyl)-*N*-phenylamino]biphenyl (NPB) and the electron transporter tris(8-hydroxylquinolino)aluminum (AlQ) were sublimed at least twice through a temperature-gradient sublimation system. Pre-patterned ITO glasses that have active device areas of 3.14 mm^2 were cleaned thoroughly by sonication in detergent, ethanol, and DI water, successively, for 5 min in each step. After being blown dry under a stream of nitrogen, the glasses were treated with oxygen plasma for 3 min and then loaded into an Ulvac Cryogenic deposition system, which was subsequently evacuated to a pressure below ca. 2×10^{-5} Torr. All of the organic layers were deposited at a rate of 1.5–2.5 Å/s. A layer of LiF (1 nm) was deposited, and then a layer of aluminum (150 nm) was deposited as the cathode. The current–voltage–luminance relationships of the devices were measured under ambient conditions using a Keithley 2400 Source meter and a Newport 1835C Optical meter equipped with an 818ST silicon photodiode. The EL spectrum was obtained using a Hitachi F4500 spectrofluorimeter. The active area of the device was 3.14 mm^2 and that of the silicon photodiode was 100 mm^2. The device was placed close to the photodiode such that all of the forward light fell on the photodiode. The external quantum efficiency was calculated according to a method described previously [17]. The luminous flux (lm) is defined [18] by $P_v = K_m \int_\lambda P_{e,\lambda} V(\lambda)\, d\lambda$, where K_m is the maximum luminous efficacy (683 lm/W), $P_{e,\lambda}$ is the spectral concentration of radiant flux, and $V(\lambda)$ is the relative photopic luminous efficiency function; the luminance (cd/m^2) is defined by luminous flux/πa, where a is the device area; the luminous efficiency (cd/A) is defined by luminous flux/πI, where I is the current; power efficiency is defined as luminous flux/IV, where V is the applied voltage.

3. Results and discussion

3.1. Synthesis and characterization

Scheme 1 illustrates the synthetic route used for the preparation of the bis(2,2-diphenylvinyl) derivative containing a spirobifluorene skeleton. Compound **1** was synthesized as described in the literature by the bromination of 1,1-diphenylethylene [15]. The lithiation of **1** with an excess of *n*-BuLi, followed by treatment with *n*-butyl borate and hydrolysis in aqueous HCl gave 2,2-diphenylvinyl boronic acid, which, without further purification, was converted to the boronic ester **2** by its reaction with pinacol. The key intermediate, 2,7-dibromo-9,9′-spirobifluorene (**3**), was prepared as reported previously by coupling the Grignard reagent obtained from 2-iodobiphenyl with 2,7-dibromo-9-fluorenone and then performing a dehydrative ring closure in acetic acid [16]. The Pd-catalyzed Suzuki coupling reaction between boronate **2** and dibromide **3** afforded the target compound, 2,7-bis(2,2-diphenylvinyl)-9,9′-spirobifluorene (**DPVSBF**) [19]. The structure of **DPVSBF** was characterized by ^{1}H and ^{13}C NMR spectroscopy. The vinylic protons give rise to a singlet at δ 6.78, while the signal for a quaternary carbon atom at δ 65.4 (C-9) indicates the presence of the spiro skeleton. High-resolution mass spectrometric and elemental analysis data provided additional verification of the proposed structure.

3.2. Thermal properties

The thermal properties of the spiro-linked bis(2,2-diphenylvinyl) derivative were investigated by differential scanning calorimetry (DSC) and thermogravimetric analysis (TGA). Fig. 1 displays the DSC curve of **DPVSBF**, which undergoes a glass transition at 115 °C, followed by crystallization at 161 °C, and finally a melting transition at 249 °C.

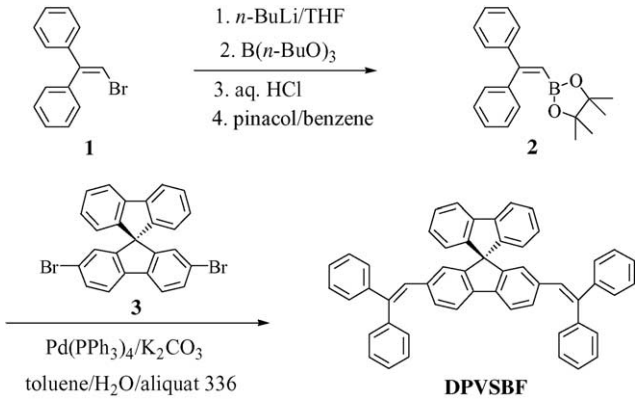

Scheme 1. Synthetic pathway of **DPVSBF**.

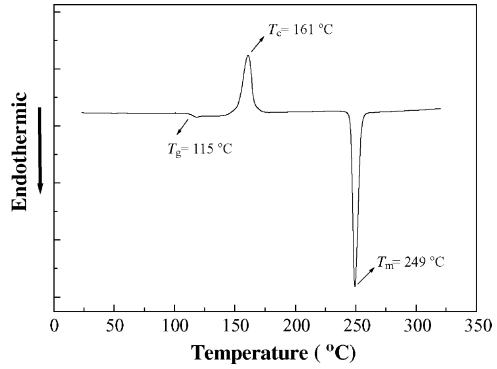

Fig. 1. DSC thermogram of **DPVSBF**.

The value of T_g exhibited by **DPVSBF** is 51° higher than that of the related analogue **DPVBi**, which undergoes its glass transition at 64 °C before crystallizing at 106 °C [7]. We attribute the enhanced morphological stability in the spirobifluorene-based material to the presence of its rigid, spiro-fused, orthogonal bifluorene linkage, which hinders the crystallization process [10,11]. The relative morphological stabilities of the two materials were further compared by microscopy. Fig. 2 shows the time-dependent optical micrograms of a vacuum-deposited **DPVBi** film. Cracks and holes were present in the film after its ambient storage for 30 min. Two days later, the whole film appeared to have crystallized. When heated at 85 °C, the morphological change was observed in less than 1 min. In contrast, no change in morphology was detected for the **DPVSBF** film after heating it at 100 °C for many hours (Fig. 3). It is important that OLEDs be constructed from materials having a relatively high value of T_g to avoid the problems associated with the presence of grain boundaries in polycrystalline films [8,9]. In addition to its high glass transition temperature, **DPVSBF** possesses high thermochemical stability, as evidenced by TGA, which indicated that the 5%-weight-loss temperature under a nitrogen atmosphere is 416 °C.

3.3. Photophysical properties

Fig. 4 depicts the solution and thin-film absorption and photoluminescence (PL) spectra of **DPVSBF**; its spectral data are summarized in Table 1. In toluene solution, **DPVSBF** possesses a lowest-energy transition with λ_{max} positioned at

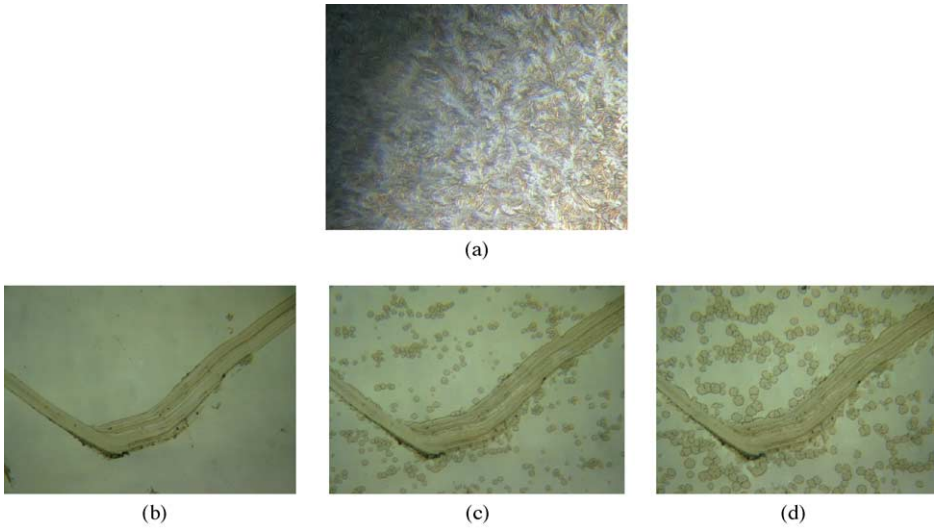

Fig. 2. Optical micrograms of a **DPVBi** film (a) kept at room temperature for 2 days, or heated at 85 °C for (b) 30 s; (c) 120 s; or (d) 240 s. A scratch was created for the purpose of providing contrast.

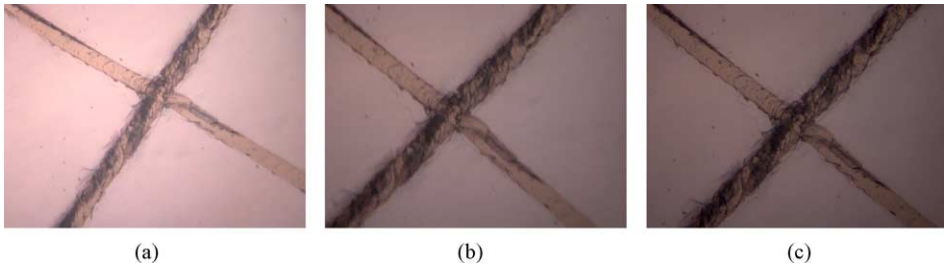

Fig. 3. Optical micrographs of a **DPVSBF** film heated at 100 °C for (a) 3 min; (b) 30 min; and (c) 3 h. The cross was created for the purpose of providing contrast.

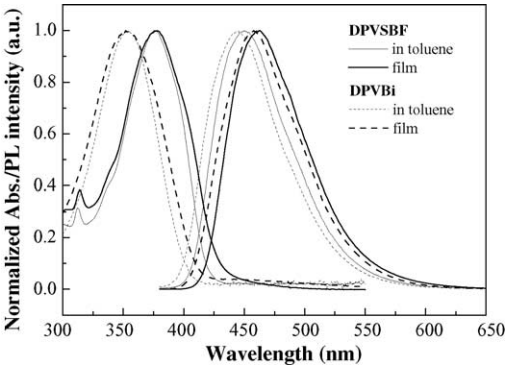

Fig. 4. UV–vis absorption and PL spectra of **DPVSBF** and **DPVBi**.

377 nm that we attribute to a π–π* transition. Upon excitation, the solution exhibits a blue PL with an emission maximum at 451 nm. The absorption band of the spirobifluorene-based molecule is moderately red-shifted (24 nm) with respect to that of its biphenyl analogue. This result indicates that the planar fluorenyl linkage plays a role in enhancing the π conjugation and reducing the HOMO–LUMO energy gap [20]. In contrast, there is only a slight red-shift (7 nm) in the PL spectra. In general, a small Stokes shift ($\lambda_{em} - \lambda_{abs}$) is expected for a molecule having a constrained geometry or existing in a confined environment because the nuclear structure of the molecule does not deviate substantially from its Franck–Condon geometry [21]. The smaller Stokes shift observed for **DPVSBF** relative to **DPVBi** is consistent with the rigid structure of the former molecule. In the case of its thin film, which we obtained by spin-coating a chloroform solution of **DPVSBF** onto a quartz plate, the absorption spectrum is almost identical to that obtained in dilute solution, but the emission maximum is red-shifted by 11–462 nm. The spectral shifts observed in the solid state probably are due to the different dielectric constants experienced in the different environments [10b].

The rigidity of the molecule also affects its excited-state lifetime and emission efficiency. In fact, we determined the excited-state lifetimes (radiative lifetimes in parenthesis) of the spiro and non-spiro molecules in toluene solutions to be 1.2 ns (1.85 ns) and 450 ps (1.90 ns), respectively; the corresponding fluorescence quantum yields (Φ_f) are 0.65 and 0.24. These values are compatible with the quantum yields – 0.73 for the former and 0.28 for the latter – determined by comparison with a fluorescence standard, 9,10-diphenylanthracene in cyclohexane ($\Phi_f = 0.90$) [22]. It is not surprising that the PL efficiency of **DPVSBF** in dilute solution is greater than that of **DPVBi** by more than a factor of 2 because twisting of the biphenyl rings may result in efficient non-radiative conversions [23]. The presence of the spiro linkage in **DPVSBF** plays a key role in inhibiting the twisting motion, which leads to its relatively longer lifetime (or larger value of Φ_f).

3.4. Electrochemistry

The electrochemical behavior of **DPVSBF** was investigated by cyclic voltammetry using ferrocene as the internal standard and the data are listed in Table 2. During the anodic scan in CH_2Cl_2, a reversible oxidation was observed at 0.73 V ($E^{\circ\prime}$) with the onset potential at 0.65 V and, thus, **DPVSBF** has a lower oxidation potential relative to that of its biphenyl analogue ($E^{\circ\prime} = 0.86$ V). Upon the cathodic sweep in THF, an irreversible reduction process was detected with an onset potential at −2.42 V, which is a value that is only slightly more negative than that of the reductive onset observed for

Table 1
Optical properties of **DPVSBF** and **DPVBi**

	Absorption, λ_{max} (nm)		PL, λ_{max} (nm)		Φ_f[a,c]	τ_{obs} (ns)[a,d]	τ_r (ns)[a,e]
	Solution[a]	Film[b]	Solution[a]	Film[b]			
DPVSBF	377	378	451	462	0.73	1.2	1.85
DPVBi	353	353	444	458	0.28	0.45	1.90

[a] In toluene.
[b] Spin-coated from their $CHCl_3$ solutions.
[c] The relative quantum yield was measured with reference to 9,10-diphenylanthracene in cyclohexane ($\Phi = 0.90$).
[d] The excited-state lifetimes.
[e] The radiative lifetimes.

Table 2
Electrochemical properties of **DPVSBF** and **DPVBi**

	E^{ox}_{onset} (V)[a]	E^{red}_{onset} (V)[a]	HOMO[b] (eV)	LUMO[c] (eV)	E^{el}_g (eV)[d]	E^{opt}_g (eV)[e]
DPVSBF	0.65	−2.42	−5.45	−2.38	3.07	2.94
DPVBi	0.79	−2.39	−5.59	−2.41	3.18	3.07

[a] Potential values are given vs. Fc/Fc^+.
[b] Determined from the onset oxidation potential.
[c] Determined from the onset reduction potential.
[d] Electrochemical band gap estimated using $E^{el}_g = E^{ox}_{onset} - E^{red}_{onset}$.
[e] Optical band gap, calculated from the absorption edge of the UV–vis spectrum.

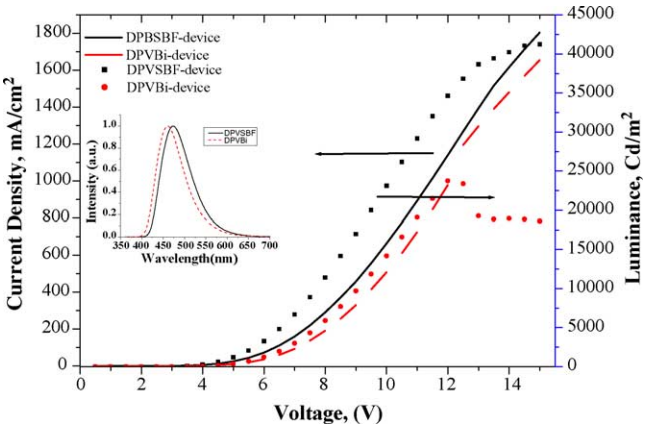

Fig. 5. Current–voltage–luminance curves for the **DPVSBF**- and **DPVBi**-based devices.

DPVBi (−2.39 V). The HOMO and LUMO energy levels of **DPVSBF** estimated from the onset potentials for the oxidation and reduction processes, respectively, are −5.45 and −2.38 eV with respect to the energy level of the ferrocene reference (4.8 eV below the vacuum level) [24]. The band gap of **DPVSBF** (3.07 eV) estimated from these electrochemical measurements is smaller than that determined for **DPVBi** (3.17 eV). Again, this feature is due to the planarity of the fluorene core: the enhanced π conjugation between the two diphenylvinyl moieties leads to the reduced band gap energy [25].

3.5. Electroluminescent properties

We fabricated light-emitting devices of the structure ITO/NPB (40 nm)/**DPVSBF** (10 nm)/AlQ (30 nm)/LiF (1 nm)/Al (150 nm), where NPB and AlQ refer to 4,4′-bis[*N*-(1-naphthyl)-*N*-phenylamino]biphenyl and tris(8-hydroxyquinoline) aluminum(III), respectively. As expected, a bright blue emission was observed with a λ_{max} at 474 nm (CIE coordinates: 0.16, 0.24). Fig. 5 shows the *I–V–L* characteristics. At a driving current of 100 mA (6.4 V), a luminance of 4110 cd/m^2 was obtained with an external quantum efficiency of 2.54%, luminance efficiency of 4.1 cd/A, and power efficiency of 2.0 lm/W. A maximum brightness of >40,000 cd/m^2 was reached at a driving voltage of 15 V. For comparison, a similar device with **DPVBi** as the emission layer was also prepared under the same conditions. This device gave a λ_{max} at 460 nm (CIE coordinates: 0.16, 0.17) and a similar external quantum efficiency (2.38%) relative to the previous device. The luminance efficiency and power efficiency are lower by ca. 30% than that based on **DPVSBF**. The higher luminance efficiency of the **DPVSBF**-based device, relative to that of the **DPVBi**-based device, might also be due to a red shift of the EL spectrum, so that it occurs closer to the maximum of the relative photopic luminous efficiency function [26]. We also note that, for the **DPVBi**-based device, a fast drop in luminance occurred at driving voltages higher than 12 V. The performance characteristics for the two devices are listed in Table 3. The major difference observed upon introducing this higher-T_g, morphologically-more-stable derivative appears to be the device's lifetime. The lifetime of a device involves many parameters, including the stability of the materials, the quality of the ITO substrate, and the encapsulation technique used. Thus, we performed a relative duration test on the devices made from **DPVSBF** and **DPVBi** under otherwise identical preparation condition. The devices were driven at the constant current at which their initial luminance was 10,000 cd/m^2. The luminance was monitored until half of the original luminance was reached. Fig. 6 shows the time-dependent luminance decay of the two devices. The device based on **DPVSBF** had a half-life of 1280 min, or a projected half-life [27] of 2133 h at a initial luminance of 100 cd/m^2. In contrast, the device based on **DPVBi** had a half-life of 78 min, and a projected half-life of 130 h at initial brightness of 100 cd/m^2. Thus, there was a 16-fold enhancement in the lifetime of the **DPVSBF** device. This improvement may be due to the higher efficiency of the **DPVSBF**-based device (so that a lower driving voltage can be applied for the same initial luminance), and/or a more stable morphology of the film materials. Because the **DPVBi** film tends to crystallize quickly, its crystallization can lead to an inhomogeneous film surface that may cause nano- or micro-scale insulating and, thus, dark spots.

Table 3
Performances of **DPVSBF**- and **DPVBi**-based devices

Brightness (cd/m^2)	η_{ext} (%)	Lum. eff. (Cd/A)	Power eff. (lm/W)	V_{drive} (V)	$V_{turn\text{-}on}$ (V)	Peak/FWHM (nm)	CIE (x, y)
DPVSBF							
928[a]	2.87[a]	4.67[a]	2.04[a]	4.82[a]	2.7	474/82	0.16, 0.24
4108[b]	2.54[b]	4.12[b]	3.05[b]	6.37[b]			
41247[c]	3.03[c]	5.33[c]	4.76[c]				
DPVBi							
714[a]	2.62[a]	3.57[a]	2.03a	5.52a	3.3	460/76	0.16, 0.17
3238[b]	2.38[b]	3.24[b]	1.44[b]	7.08[b]			
23753[c]	3.01[c]	4.12[c]	3.5[c]				

[a] Values recorded at 20 mA/cm^2.
[b] Values recorded at 100 mA/cm^2.
[c] Maximum values of the devices.

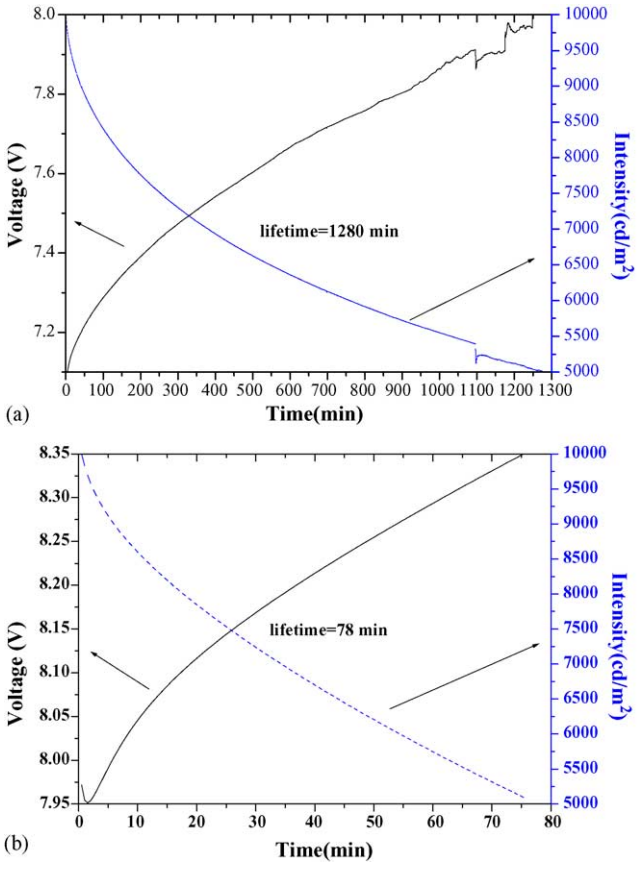

Fig. 6. Tests of the stability of (a) the **DPVSBF**-based and (b) **DPVBi**-based devices. The devices were driven at the constant current that provided an initial luminance of 10,000 cd/m^2.

4. Conclusions

We have prepared a new blue emitter, **DPVSBF** that possesses most of the photophysical and electronic properties of **DPVBi**, but has a higher glass transition temperature as a result of the presence of its spirobifluorene linking group. In comparison with the corresponding tetrasubstituted derivative **Spiro-DPVBi** [13], **DPVSBF** is highly sublimable, which is most advantageous for device fabrication. This material also has a much longer operation lifetime, relative to that of **DPVBi**, when incorporated into an electroluminescent device; this property makes **DPVSBF** a more practical material. In a standard three-layer configuration and at a driving current of 100 mA (6.4 V), the device exhibited a luminance of 4110 cd/m^2 with an external quantum efficiency of 2.54%, a luminance efficiency of 4.1 cd/A, and a power efficiency of 2.0 lm/W.

Acknowledgement

Financial support from both the National Science Council of Taiwan and the Academia Sinica, Taiwan, is gratefully acknowledged.

References

[1] C.W. Tang, S.A. Van Slyke, Appl. Phys. Lett. 51 (1987) 913.
[2] S. Miyata, H.S. Nalwa (Eds.), Organic Electroluminescent Materials and Devices, Gordon and Breach Publishers, New York, 1997.
[3] (a) C.H. Chen, J. Shi, C.W. Tang, Coord. Chem. Rev. 171 (1998) 161;
(b) U. Mitschke, P. Bäuerle, J. Mater. Chem. 10 (2000) 1471;
(c) L.S. Hung, C.H. Chen, Mater. Sci. Eng. R 39 (2002) 143.
[4] (a) J. Kido, K. Hongawa, K. Okuyama, K. Nagai, Appl. Phys. Lett. 64 (1994) 815;
(b) J. Kido, H. Shionoya, K. Nagai, Appl. Phys. Lett. 67 (1995) 2281;
(c) F.C. Chen, Y. Yang, M.E. Thompson, J. Kido, Appl. Phys. Lett. 80 (2002) 2308.
[5] (a) C. Hosokawa, H. Higashi, H. Nakamura, T. Kusumoto, Appl. Phys. Lett. 67 (1995) 3853;
(b) S.E. Shaheen, G.E. Jabbour, M.M. Morrell, Y. Kawabe, B. Kippelen, N. Peyghambarian, M.-F. Nabor, R. Schlaf, E.A. Mash, N.R. Armstrong, J. Appl. Phys. 84 (1998) 2324.
[6] (a) Y.-S. Huang, J.-H. Jou, W.-K. Weng, J.-M. Liu, Appl. Phys. Lett. 80 (2002) 2782;
(b) K.O. Cheon, J. Shinar, Appl. Phys. Lett. 81 (2002) 1738;
(c) G. Li, J. Shinar, Appl. Phys. Lett. 83 (2003) 5359;
(d) X.Y. Zheng, W.Q. Zhu, Y.Z. Wu, X.Y. Jiang, R.G. Sun, Z.L. Zhang, S.H. Xu, Displays 24 (2003) 121;
(e) W. Xie, J. Hou, S. Liu, Semicond. Sci. Tech. 18 (2003) 42;
(f) W. Xie, S. Liu, Y. Zhao, J. Phys. D: Appl. Phys. 36 (2003) 1246.
[7] S. Wang, W.J. Oldham Jr., R.A. Hudack Jr., G.C. Bazan, J. Am. Chem. Soc. 122 (2000) 5695.
[8] M.D. Joswick, I.H. Cambell, N.N. Barashkov, J.P. Ferraris, J. Appl. Phys. 80 (1996) 2883.
[9] (a) S. Tokito, H. Tanaka, K. Noda, A. Okada, Y. Taga, Appl. Phys. Lett. 70 (1997) 1929;
(b) B.E. Konne, D.E. Loy, M.E. Thompson, Chem. Mater. 10 (1998) 2235;
(c) D.F. O'Brien, P.E. Burrows, S.R. Forrest, B.E. Konne, D.E. Loy, M.E. Thompson, Adv. Mater. 10 (1998) 1108;
(d) F. Steuber, J. Staudigel, M. Stössel, J. Simmerer, A. Winnacker, H. Spreitzer, F. Weissörtel, J. Salbeck, Adv. Mater. 12 (2000) 130;
(e) Y. Shirota, J. Mater. Chem. 10 (2000) 1.
[10] (a) J. Salbeck, J. Bauer, F. Weissörtel, Macromol. Symp. 125 (1997) 121;
(b) J. Salbeck, N. Yu, J. Bauer, F. Weissörtel, H. Bestgen, Synth. Met. 91 (1997) 209;
(c) N. Johansson, D.A. dos Santos, S. Guo, J. Cornil, M. Fahlman, J. Salbeck, H. Schenk, H. Arwin, J.L. Brédas, W.R. Salenek, J. Chem. Phys. 107 (1997) 2542;
(d) N. Johansson, J. Salbeck, J. Bauer, F. Weissörtel, P. Bröms, A. Andersson, W.R. Salaneck, Adv. Mater. 10 (1998) 1136;
(e) H. Tian, B. Chen, P.H. Liu, Chem. Lett. (2001) 990;
(f) W.J. Shen, R. Dodda, C.C. Wu, F.I. Wu, T.H. Liu, H.H. Chen, C.H. Chen, C.F. Shu, Chem. Mater. 16 (2004) 930;
(g) C.H. Chen, F.I. Wu, C.F. Shu, C.H. Chien, Y.T. Tao, J. Mater. Chem. 14 (2004) 1585.
[11] C.C. Wu, Y.T. Lin, H.H. Chiang, T.Y. Cho, C.W. Chen, K.T. Wong, Y.L. Liao, G.H. Lee, S.M. Peng, Appl. Phys. Lett. 81 (2002) 577.
[12] R. Wu, J.S. Schumm, D.L. Pearson, J.M. Tour, J. Org. Chem. 61 (1996) 6906.
[13] (a) H. Spreitzer, H. Schenk, J. Salbeck, F. Weissöertel, H. Riel, W. Riess, Proc. SPIE-Int. Soc. Opt. Eng. 3797 (1999) 316;
(b) H. Spreitzer, H. Vestweber, P. Stößel, H. Becker, Proc. SPIE-Int. Soc. Opt. Eng. 4105 (2001) 125.
[14] H. Tokailin, H. Higashi, C. Hosokawa, US Patent 5 130 630 (1992).
[15] S.M. Korneev, D.E. Kaufmann, Synthesis (2002) 491.
[16] J. Pei, J. Ni, X.H. Zhou, X.Y. Cao, Y.H. Lai, J. Org. Chem. 67 (2002) 4924.

[17] S.R. Forrest, D.D.C. Bradley, M.E. Thompson, Adv. Mater. 15 (2003) 1043.
[18] G. Wyszecki, W.S. Stiles, Color Science: Concepts and Methods, Quantitative Data and Formulae, John Wiley & Sons, New York, 1982, p. 259.
[19] N. Miyaura, A. Suzuki, Chem. Rev. 95 (1995) 2457.
[20] K.T. Wong, Z.J. Wang, Y.Y. Chien, C.L. Wang, Org. Lett. 3 (2001) 2285.
[21] J.R. Lakowicz, Principles of Fluorescence Spectroscopy, second ed., KA/PP, New York, 1999, pp. 185–236, Chapters 6–7, and other related references cited therein.
[22] D. Eaton, Pure Appl. Chem. 60 (1998) 1107.
[23] N.J. Turro, Modern Molecular Photochemistry, University Science Books, Sausalito, CA, 1991, pp. 170–172.
[24] J. Pommerehne, H. Vestweber, W. Guss, R.F. Mahrt, H. Bässler, M. Porsch, J. Daub, Adv. Mater. 7 (1995) 551.
[25] D.E. Loy, B.E. Konne, M.E. Thompson, Adv. Funct. Mater. 12 (2002) 245.
[26] According to the definition of luminous flux [17] [i.e., $P_{\mathrm{v}} = K_{\mathrm{m}} \int_{\lambda} P_{\mathrm{e},\lambda} V(\lambda)\,\mathrm{d}\lambda$], the closer the maximum of the EL is to the relative photopic luminous efficiency function, the higher the luminous flux.
[27] S.A. Van Slyke, C.H. Chen, C.W. Tang, Appl. Phys. Lett. 69 (1996) 2160.